

Enhanced nonlinear optical and optical limiting responses of 7-diethylamino-4-methyl coumarin functionalized with silver nanoparticles: A combined experimental and DFT study

Shradha Lakhera^a, Meenakshi Rana^{a,*}, Vivek Dhuliya^b, L.P. Purohit^b, A. Dhanusha^c, T.C. Sabari Girisun^c

^a Department of Physics, School of Sciences, Uttarakhand Open University, Haldwani 263139, Uttarakhand, India

^b Department of Physics, Gurukul Kangri (Deemed to be University), Haridwar 249404, Uttarakhand, India

^c Nanophotonics Laboratory, Department of Physics, Bharathidasan University, Tiruchirappalli, Tamil Nadu 620024, India

ARTICLE INFO

Keywords:

Density functional theory
7-diethylamino-4-methyl coumarin
Silver
Nanoparticles

ABSTRACT

The present study accounts for the enhanced nonlinear optical and optical limiting activity of 7-diethylamino-4-methyl coumarin (7DMC) after the addition of silver nanoparticles. The theoretical calculations were done in three different solvents water, methanol, and dimethyl formamide (DMF), and on the basis of the energy gap, DMF was selected as the most suitable solvent. Further, the liquid samples were prepared in DMF. The natural bond orbitals show the active participation of the lone pairs of electrons of 2O and 35Ag as donor and acceptor moieties respectively. The values of first-order hyperpolarizability of the 7DMC+Ag₃ combination were raised to 2002.71×10^{-30} esu, 778.72×10^{-30} esu, and 677.12×10^{-30} esu in water, methanol, and DMF. The valley-like structure in the Z-Scan spectra indicated the occurrence of reverse saturable absorption in the prepared samples. The optical limiting threshold of the 7DMC+AgNps was decreased from that of the probe 7DMC and AgNps indicating the early attenuation of the optical limiting nature of the combination. Thus, the overall results validated the enhanced optical nonlinearity of the combination. Moreover, it can be stated that the proposed nanoparticles combination 7DMC+AgNps has potential candidature to be used for the fabrication of laser safety devices and eye aids.

1. Introduction

During the last two decades, nonlinear optical (NLO) materials have attained much consideration. With the vast potential applications in optical switching, telecommunications, molecular switches, dynamic holography, and many more, NLO materials have been a very contemporary sector of research [1,2]. The discovery of NLO materials has eased us not only with deep insights into light-matter interactions but also NLO materials that are potentially nonlinear has been established in almost every type of media like solids, films, pellets, solutions, and many more [3,4]. The literature presents that among different kinds of materials, organic materials are the one that provides the best medium for optical nonlinearities [5]. The flexible, user-friendly, strong intramolecular charge transfer (ICT), and non-hazardous nature of the organic systems make them a potential target to work with [6].

Researchers have explored many kinds of organic materials with immense NLO responses. Density functional theory (DFT), on the other hand has become a most widely employed quantum chemical calculation tool. It is known for its robust and accurate results and hence used in numerous studies for reporting different opto-electronic properties. There are several studies reported in the literature where DFT has been employed for theoretical modelling. Some organic and hybrid families with large optical nonlinearities are imidazole [7], coumarins [8,9], quinolines [10], tetraphenylethylene compounds [11], fatty alcohols [12], amino acids [13], organic dyes [14], hydrocarbons [15], polymers [16], toluenes [17], pyrenes [18], pyrrole [19], fullerenes [20], butanamide [21], Salicylaldehyde [22], drugs [23], cyanoacrylic acid [24] and many more. The derivatives of these kinds of compounds have attained popularity in varied NLO applications like data storage, optical limiting, harmonic generation, etc.

* Corresponding author.

E-mail address: mrana@uou.ac.in (M. Rana).

¹ 0000-0002-9156-9125.

<https://doi.org/10.1016/j.jphotochem.2024.115910>

Received 22 May 2024; Received in revised form 19 July 2024; Accepted 22 July 2024

Available online 23 July 2024

1010-6030/© 2024 Elsevier B.V. All rights are reserved, including those for text and data mining, AI training, and similar technologies.

In the applications related to microfabrication, the large structures of organic systems create challenges for the researchers. Nanomaterials, on the other hand, have proven advantageous in such cases. It is found that the nanomaterials and nanocomposites exhibit large NLO responses. The minimal size of the nano range (10^{-9} m) provides flexibility in micro-fabrication and thus the small size of the nanomaterials makes them suitable for a variety of nonlinear optical applications [25]. Apart from the probe organic systems, researchers have also investigated the optical nonlinearity of the combination of organic systems and nanoparticles (Nps). There are many studies in the literature that yield large values of hyperpolarizability coefficients for nanomaterials. The gold nano-clusters were computationally investigated by S. Knoppe and it was found that the first-order hyperpolarizability of the Au_{25} cluster was obtained as 44.7×10^{-30} esu [26]. A study done by U.R. Felscia and the team demonstrated the optical nonlinearity of the quinacridone combined with silver and gold nanoparticles [27]. The referenced study gave higher values for quinacridone adsorbed with silver trimer (Ag_3) as 930×10^{-30} esu and quinacridone adsorbed with gold trimer (Au_3) as 120×10^{-30} esu [27]. A similar kind of work was done on one more quinacridone derivative namely 2,9-dimethyl quinacridone (2,9-DMQA) in which the values of first-order hyperpolarizability for 2,9-DMQA adsorbed with Ag_3 and Au_3 was obtained as 1163×10^{-30} and 1066×10^{-30} esu respectively [28]. One more study was reported by U.R. Felscia in which the authors have done a theoretical investigation of the increased first-order hyperpolarizability of aromatic compounds like chrysene, tetraphene, tetra helicene, pyrene, and triphenylene adsorbed with Ag_3 [29]. The calculated values of first-order hyperpolarizabilities for Chr- Ag_3 , TeH- Ag_3 , TeP- Ag_3 , TrP- Ag_3 , and Py- Ag_3 were found to be 261×10^{-30} , 331×10^{-30} , 432×10^{-30} , 206×10^{-30} , and 435×10^{-30} esu respectively. These values were much higher compared to those of the probe compounds and the introduction of the Ag_3 was found successful in enhancing the NLO activity [29]. Author Y. Chang and his team demonstrated the anisotropic polarizability of silver nanoclusters composed of fourteen silver atoms between the range 69.5×10^{-24} to 1493×10^{-24} esu [30]. The adsorption of the Ag_3 and Au_3 on the organic molecule pentacene-2,5-dione (PD) have also been investigated [31]. The high value of hyperpolarizability for PD- Ag_3 (184.22×10^{-30} esu) and PD- Au_3 (2057.26×10^{-30} esu) supported their potential applications in highly efficient NLO devices [31]. Such kinds of metal-organic combinations have also been employed for various optoelectronic properties, especially in sensing. A study reported the interesting enhancement of the first-order hyperpolarizability of Ag_3 adsorbed nitropyrene (2071.630×10^{-30} esu) as compared to probe nitropyrene (15.05×10^{-30} esu) [32]. Further, the designed combination was used for metal ion sensing applications, and mercury detection was estimated in the reported study [32]. Our previously done research work on the computational hyperpolarizability of *para*-aminobenzoic acid adsorbed with Ag_3 also supports the present study [33]. The first-order hyperpolarizability of *para*-aminobenzoic acid adsorbed with Ag_3 was calculated as 14769.05×10^{-30} , 14545.83×10^{-30} , 14590.86×10^{-30} , and 14657.17×10^{-30} esu in water, methanol, dimethyl formamide, and dimethyl sulfoxide mediums [33]. These values support the extraordinary NLO responses of *para*-aminobenzoic acid combined with Ag_3 . There are a lot of such studies in the literature reporting the metal-molecule interactions and their intensified NLO properties.

Previously, we have done experimental demonstrations of the NLO activity and optical limiting activity of probe 7-diethylamino-4-methyl coumarin (7DMC), and the results were very satisfying in establishing the optical limiting (OL) characteristics of 7DMC [34]. On the other hand, literature suggests that silver nanoparticle ($AgNps$) is the best dopant to escalate the optical nonlinearity of the compounds. The present study is the connective work of the previously done research work on the NLO activity and laser limiting activity of 7DMC. The theoretical studies of NLO activity were done on 7DMC+ Ag_3 and further supported by the experimental results found for 7DMC+ $AgNps$. The natural charge distribution and bond orbital study established the intermolecular

interactions between the 7DMC and trimer. The charge surfaces as molecular electrostatic potential (MEP) surfaces, molecular isosurfaces, transition density matrix (TDM) plots, counterplots, and electron localization function (ELF) surfaces were used to identify the nucleophilic and electrophilic parts of the 7DMC+ Ag_3 combination. The chemical reactivity parameters were obtained for proving the responses to the global reactivity descriptors. The absorption and vibrational spectra were computed for 7DMC+ Ag_3 in three considered solvents. The introduction of different solvents was done for the selectivity of the most suitable solvent for experimental work. The NLO parameters were calculated and used to theoretically estimate the NLO activity of the proposed combination. Further, the experimental counterpart of the theoretical results was done with the liquid sample prepared with 7DMC combined with $AgNps$. The results of the absorption and vibrational spectra for these samples were experimentally obtained and compared with the theoretical spectroscopic results. The NLO and OL activity of 7DMC+ $AgNps$ was tested with the help of Z-Scan spectroscopy. The reported combined computational and experimental study brings the potential characteristics of the 7DMC+ $AgNps$ combination for optical power limiting applications.

2. Materials and methods

2.1. Theoretical methods

The probe structure of 7DMC downloaded from the database PubChem (CID:7050) (<https://pubchem.ncbi.nlm.nih.gov/>) was first optimized by imposing no geometrical restrictions. As 7DMC is soluble in water, methanol, and dimethyl formamide (DMF), these three solvents were considered for computational analysis and based on the lowest value of the E_g , most suitable solvent was considered as the solvent for experiments. The integral equation formalism-polarizable continuum model (IEF-PCM) model with the self-consistent reaction field (SCRF) method was followed for performing the calculations in the solvent phases. Gaussian 09 software (<https://gaussian.com>) was used for all the quantum chemical calculations and the Gauss view program (<https://gaussian.com/gaussview6/>) was used for the visualizations [35,36]. The builder tool in the Gaussian was used to draw the geometry of the silver trimer (Ag_3) near the reactive site of the 7DMC molecule to obtain maximum interaction between the trimer and 7DMC. It is known that silver trimer is the primary state of the nucleation of the Ag. This makes Ag_3 the most stable form of Ag and thus it can be considered as the nanoparticle form of silver [37]. For the 7DMC+ Ag_3 combination, the B3PW91/LANL2DZ method was used for the optimization calculations. The mentioned set of functions was most profoundly used for studying the metal-molecule contact and interactions [26–30]. The “Dispersion energy = Grimme GD3” method was used for calculating the empirical dispersion term for the combination [38,39]. The electronic energy ($E_{\text{electronic}}$) and thermal energy (E_{thermal}) was used for calculating the free energy of 7DMC+ Ag_3 combination by equation (1):

$$E_{\text{free}} = E_{\text{electronic}} + E_{\text{thermal}} \quad (1)$$

Interaction energy for the 7DMC+ Ag_3 combination was calculated using the expression (2):

$$E_{\text{int}} = E_{\text{complex}} - (E_{7\text{DMC}} + E_{Ag_3}) \quad (2)$$

Koopman's set of equations was used for calculating the global reactivity descriptors [39]. As per Koopman, IP and EA are nearly equivalent to the negative energy of the HOMO and LUMO energies [40]. The energies of the highest occupied and lowest unoccupied molecular orbitals (HOMO and LUMO) were used for the calculations of the reactivity parameters. Different reactivity parameters like energy gap (ΔE), ionization potential (IP), electron affinity (EA), chemical potential (CP), electronegativity (χ), and electrophilicity (ω) [28,31,41] are calculated using equations given below:

$$\Delta E = E_{LUMO} - E_{HOMO} \quad (3)$$

$$IP = -E_{HOMO} \quad (4)$$

$$EA = -E_{LUMO} \quad (5)$$

$$CP = \frac{E_{HOMO} + E_{LUMO}}{2} \quad (6)$$

$$\chi = \frac{(IP + EA)}{2}, \quad (7)$$

$$\omega = \frac{\mu^2}{2\eta} \quad (8)$$

$$\omega^+ = \frac{(IP + 3EA)^2}{16(IP - EA)} \quad (9)$$

$$\omega^- = \frac{(3IP + EA)^2}{16(IP - EA)} \quad (10)$$

The natural bond orbital (NBO) analysis was done to analyze the quantitative charge transfer in the 7DMC+Ag₃ combination [42,43]. The stabilization energy ($E(2)$) was calculated using second-order perturbation theory for each donor (i) and acceptor (j) atom. The $E(2)$ corresponding to the delocalization of each $i \rightarrow j$ was calculated using the expression:

$$E(2) = \Delta E_{ij} - q_i \left(\frac{f_{ij}^2}{E_j - E_i} \right) \quad (11)$$

where $F(i,j)$ is the Fock matrix element between i and j NBO orbitals, ΔE_{ij} is the energy corresponding to each NBO interaction, and E_j and E_i are the energies of the acceptor and donor NBOs. The quantitative value of the net transferred charge from donor to acceptor moieties was predicted by inter-fragment charge transfer (IFCT) analysis. The IFCT analysis was obtained from Multiwfn software (<https://sobereva.com/multiwfn/>) [44]. Density of states (DOS) spectra were plotted for 7DMC+Ag₃ combination in water, methanol, and DMF for verifying the obtained band gap. The DOS spectra were obtained using Gauss sum software (<https://gausssum.sourceforge.net/>) [45]. The TDM and ELF analysis was reported using Multiwfn software. The ELF and MEP surfaces were used for identifying the nucleophilic and electrophilic moieties in the 7DMC+Ag₃ combination. The time-dependent density functional theory (TD-DFT) was used for calculating the UV-Vis spectra. The absorption spectra were recorded for the 7DMC+Ag₃ combination for nine transitions and the details of the electronic transitions were retrieved from the obtained spectra. The polar calculations were done using the finite field theory approach for obtaining the vibrational details. Fourier transfer infrared spectra (FT-IR) were obtained for the 7DMC+Ag₃ combination in water, methanol, and DMF. Polar calculations were further used for obtaining the tensor components of NLO parameters such as total dipole moment (μ_{total}), total isotropic polarizability (α_{total}), anisotropic polarizability ($\Delta\alpha$), and first-order hyperpolarizability (β_{total}). Values of α_{xx} , α_{yy} , and α_{zz} (tensor components of polarizability) and β_{xxx} , β_{yyy} , β_{zzz} , β_{xyy} , β_{xzz} , β_{yzz} , β_{yxx} , β_{zxx} , and β_{zyy} (tensor components of hyperpolarizability). These parameters are the computed using following expression:

$$\mu_{tot} = \left(\mu_x^2 + \mu_y^2 + \mu_z^2 \right)^{\frac{1}{2}} \quad (12)$$

$$\alpha_{total} = \frac{1}{2} (\alpha_{xx} + \alpha_{yy} + \alpha_{zz}) \quad (13)$$

$$\Delta\alpha = \frac{1}{\sqrt{2}} \left[(\alpha_{xx} - \alpha_{yy})^2 + (\alpha_{yy} - \alpha_{zz})^2 + (\alpha_{zz} - \alpha_{xx})^2 + 6\alpha_{xz}^2 + 6\alpha_{xy}^2 + 6\alpha_{yz}^2 \right]^{\frac{1}{2}} \quad (14)$$

$$\beta_{total} = \left[(\beta_{xxx} + \beta_{xyy} + \beta_{xzz})^2 + (\beta_{yyy} + \beta_{yzz} + \beta_{yxx})^2 + (\beta_{zzz} + \beta_{zxx} + \beta_{zyy})^2 \right]^{\frac{1}{2}} \quad (15)$$

2.2. Experimental methods

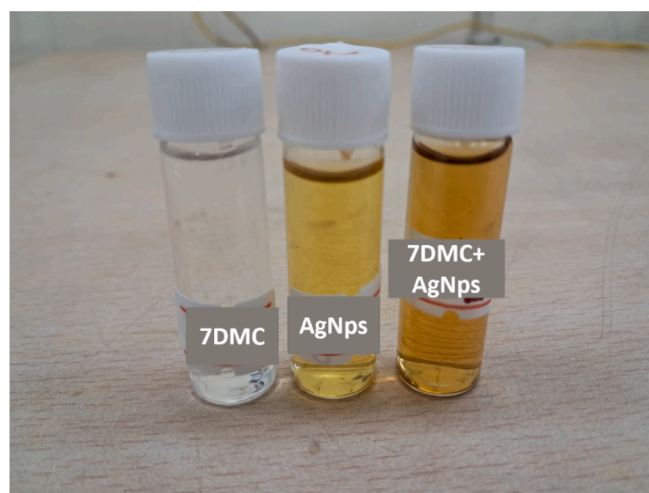
The colloidal solution of AgNPs was prepared using Creighton's method as discussed in previously reported studies [32]. AgNO₃ was used as a precursor and NaBH₄ was used as a reducing agent. Both AgNO₃ and NaBH₄ solutions were prepared of 1 mM concentration and pre-cooled to ice temperature. In a beaker, 7.5 ml of AgNO₃ was added dropwise (one drop per second) to 22.5 ml of NaBH₄, and the reaction was carried out in an ice bath with continuous stirring. The stirring was stopped on the complete addition of AgNO₃ to NaBH₄. A gradual change in the color of the solution from colorless to yellow confirmed the formation of AgNps.

Same method as followed for the preparation of the AgNps was followed for the preparation of the AgNps combined 7DMC. Liquid 7DMC (4 ml) was added dropwise to the AgNO₃ solution in an ice bath with continuous stirring. The stirring was stopped as soon as the 7DMC was added completely. After this, the prepared solution was immediately added to the NaBH₄ dropwise in an ice bath and stirred till the solution was completely added. The prepared solution was the organic compound doped with AgNps (Scheme 1).

The UV-Vis absorption spectroscopy of 7DMC, AgNps, and 7DMC+AgNps was performed using Perkin-Elmer model Lambda-35 absorption spectrophotometer with tungsten iodide and deuterium light source and spectra was traced in a general absorption range of 200–1100 nm and varying slit width of 0.5 and 1.0 nm. The data obtained from the absorption spectra was further used for the calculation of the band gap (ΔE). Mott and Davis's relationship was used for calculating ΔE :

$$(ah\nu)^{\gamma} = A(h\nu - \Delta E) \quad (16)$$

The identification of the available functional groups after the mixing of two compounds was done using a FT-IR spectrophotometer. A Perkin-Elmer FT-IR spectrophotometer of model Spectrum BX-II with nichrome glower wire light source and a DTGS detector was used to get the vibrational details for each of the samples. The open-aperture Z-scan spectroscopy with a nano-pulsed Nd: YAG laser beam of 17 μ m waist, 532 nm wavelength, 15 cm focal length, and 10 Hz frequency was used to get the relationship between normalized transmittance (β) and Z . The theoretical data fitting to get the proper curve between β and Z . Sheik-Bahae formalism mentioned below (2) was employed to calculate the



Scheme 1. Prepared liquid samples of probe 7DMC, AgNps, and 7DMC+AgNps.

nonlinear absorption coefficient (β).

$$\frac{dI}{dz} = \left[\frac{\alpha_0}{1 + \frac{I}{I_s}} + \beta I \right] I \quad (17)$$

where α_0 is unsaturated linear absorption at the excitation, I is input intensity of the laser, I_s is saturation intensity, and Z is the samples propagation distance.

The linear transmittance (L_T) was calculated using the input (P_0) and output power (P) with the expression mentioned in (3):

$$L_T = \frac{P}{P_0} \quad (18)$$

The linear absorption coefficient (α_0) was computed using L_T and considering the 1 mm sample thickness (1 mm) by equation mentioned in (4):

$$\alpha_0 = - \left(\frac{1}{L} \right) \ln \left(\frac{P}{P_0} \right) \quad (19)$$

3. Results and discussion

3.1. Structural and adsorption analysis

Fig. 1 illustrates the optimized geometry of the 7DMC+Ag₃ combination. The molecule 7DMC has one nitrogen 3 N, and two oxygen 1O, and 2O atoms that majorly contribute to the intramolecular charge transfer and lead to the stability of the 7DMC molecule. The Ag₃ trimer was at the bond length of 2.2 Å from the 2O atom of the 12C=2O group. The bond length of the 17C=2O bond was also increased from 1.22 Å (in probe 7DMC) to 1.25 Å after the formation of the 7DMC+Ag₃ combination and this further increases to 1.26 Å for methanol and DMF. The dispersion energy, free energy, and interaction energy of the 7DMC+Ag₃ combination in water, methanol, and DMF are listed in Table 1. Negative values were obtained for the interaction energy of the 7DMC+Ag₃ combination for all the solvents. The negative interaction energy indicates the release of energy for the bond formation between the probe 7DMC and the trimer [46]. The exothermic reaction between both moieties was also supported by the negative value of the free energy in each solvent. Moreover, it also supports the existence of attractive forces between probe 7DMC and the trimer. Therefore, the adsorption parameters and the calculated energies suggest the possible adsorption of the trimer on the surface of the 7DMC molecule, and a strong intermolecular attraction was observed between both the moieties. Additionally, the comparison of the $E_{\text{dispersion}}$, E_{free} , and $E_{\text{interaction}}$ suggested that DMF was the most suitable solvent for 7DMC+Ag₃.

3.2. Molecular orbitals and density of states analysis

The DOS spectra illustrated in Fig. 2 were computed to obtain the

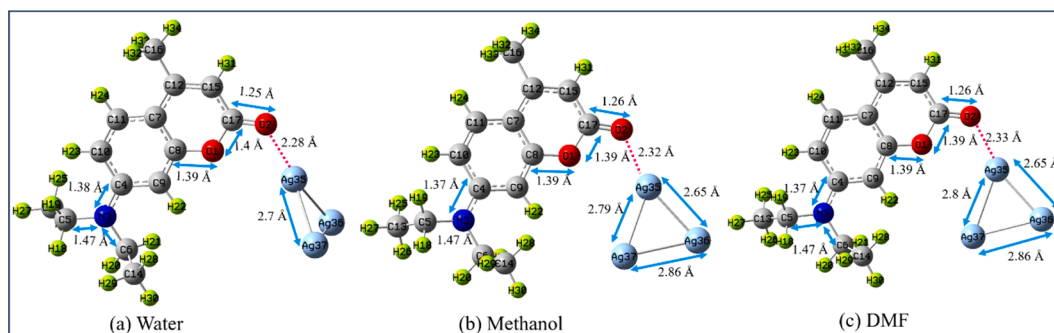


Fig. 1. Optimized geometry of 7DMC+Ag₃ combination.

Table 1

$E_{\text{dispersion}}$, E_{free} , and $E_{\text{interaction}}$ of 7DMC+Ag₃ combination in solvents water, methanol, and DMF (all energies are in kcal/mol).

Parameters	Water	Methanol	DMF
$E_{\text{dispersion}}$	-30.01	-30.16	-30.19
E_{free}	-744067.27	-744075.95	-744075.98
$E_{\text{interaction}}$	-77.37	-86.39	-77.37

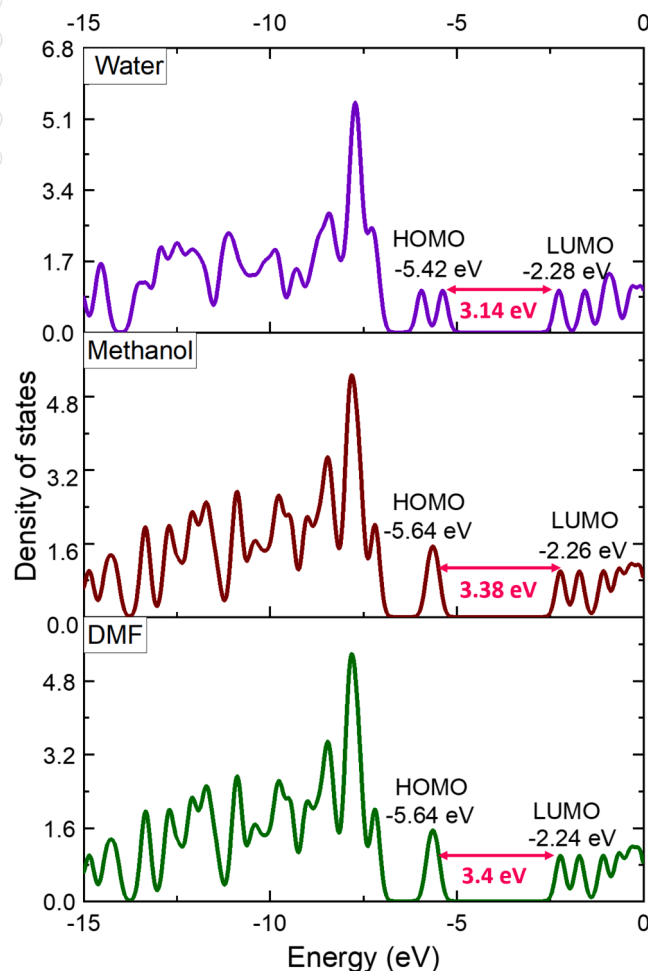


Fig. 2. Comparison of the density of states spectra of 7DMC and 7DMC+Ag₃ combination and location of the HOMO-LUMO orbitals.

energy gap of the 7DMC+Ag₃ combination. The highly accumulated peaks of the density of states on the left side of the spectra show HOMO and peaks on the right side indicate the LUMO. The energy gap of the 7DMC+Ag₃ combination in water, methanol, and DMF was computed as 3.14, 3.38, and 3.4 eV respectively. The global reactivity descriptors calculated using Koopman's equations have been listed in Table 2. The calculated energy gap of the 7DMC+Ag₃ combination using Koopman's equation was observed as 3.11, 3.32, and 3.32 eV for water, methanol, and DMF respectively. The energy gap obtained from DOS spectra was very close to the energy gap obtained by Koopman's identity. Moreover, the value of the energy gap of the 7DMC+Ag₃ combination was found to be reduced as compared to the energy gap or probe 7DMC (3.69 eV). The energy gap of the 7DMC+Ag₃ combination was also less than the experimental band gap of probe 7DMC (3.7 eV) obtained in the previously published work [29]. The reduction in the energy gap after the introduction of the trimer shows the higher possibility of the excitation of the charge from the ground state to the excited state orbitals. Thus, the introduction of the trimer reveals the increased chemical reactivity of the 7DMC+Ag₃ combination. The parameters IP and EA denote the ability of the donor and acceptor to donate and withdraw the charge cloud. The minimum value of IP shows easy donating and the higher value of EA shows easy withdrawing of the charge cloud [39]. The value of IP was reduced to 5.363 (water), 5.364 (methanol), and 5.364 eV (DMF) after the introduction of the trimer. The EA values were raised to 2.25 (water), 2.21 (methanol), and 2.21 eV (DMF). Thus, the values of IP and EA denote the increased chemical reactivity of the 7DMC+Ag₃ combination. The value of CP was also seen to decrease after the introduction of the trimer. The chemical reactivity of the molecule is addressed by χ and this value was also increased to 3.8, 3.87, and 3.87 eV for water, methanol, and DMF respectively. The chemical hardness was however reduced from the hardness of the probe 7DMC. This might be due to the introduction of the trimer. As Ag atoms are highly reactive, they are capable enough to reduce the rigidity of the combination and make it potentially flexible for participating in chemical reactions. The higher values of ω^- of the 7DMC+Ag₃ combination in all the solvents denote the dominating donor character of the Ag₃ trimer. Therefore, the overall discussion presented by the DOS spectra and the global reactivity descriptors reveals the increased chemical reactivity of the 7DMC+Ag₃ combination as compared to the probe 7DMC molecule. The lowest ΔE obtained in DMF makes it ideal solvent for performing experimental studies.

Table 2
Global reactivity parameters of probe 7DMC and 7DMC+Ag₃ combination (All values in eV).

S No.	Molecular property	7DMC	7DMC+Ag ₃ (Water)	7DMC+Ag ₃ (Methanol)	7DMC+Ag ₃ (DMF)
1.	E _{HOMO}	-5.57	-5.36	-5.53	-5.53
2.	E _{LUMO}	-1.88	-2.25	-2.21	-2.21
3.	Energy gap (ΔE)	3.69	3.11	3.32	3.31
4.	Ionization potential (IP)	5.57	5.36	5.53	5.53
5.	Electron affinity (EA)	1.88	2.25	2.21	2.21
6.	Chemical potential (CP)	-3.72	-3.80	-3.87	-3.87
7.	Electronegativity (χ)	3.72	3.80	3.87	3.87
8.	Hardness (η)	1.84	1.55	1.66	1.66
9.	Softness (S)	0.54	0.64	0.60	0.60
10.	Electrophilicity index (ω)	3.5	4.6	4.51	4.51
11.	Electron accepting power (ω^+)	2.12	2.95	2.78	2.78
12.	Electron donating power (ω^-)	5.85	6.76	6.65	6.65

3.3. Surfaces and counters

The MEP surface was mapped for the 7DMC+Ag₃ combination to get a better understanding of the charge donor and acceptor moiety. The red and blue color in the MEP surface (Fig. 3 (a)) indicates the electron-donating and electron-withdrawing groups in the combination. The blue surface over the trimer suggests the donating nature of the trimer and the red surface over the oxygen atoms of 7DMC shows the withdrawing nature of 7DMC [47]. To support the interpretation of the MEP surface, the counterplots have been plotted and illustrated in Fig. 3 (b). The denser lines of the counterplot show the accumulation of the charge cloud. The lightly dense counter lines around the Ag₃ show that the trimer has donated the charge cloud and there is a lack of charge over the trimer. On the other hand, the charge cloud was observed over the 7DMC molecule. The molecular isosurface illustrated in Fig. 3 (c) shows the green isosurface over the 7DMC. These isosurfaces are the indication of the charge cloud. Therefore, the MEP surface, isosurface, and counterplots validate the charge transportation from the trimer toward the 7DMC molecule.

3.4. Transition density matrix and electron localization function surface analysis

The ELF surface shown in Fig. 4 (a) is the interpretation of the localization of the charge available over the geometry. The red spots show the presence of the charge cloud. The ELF surface is in good agreement with the MEP surface. There were no such red spots over the Ag₃ trimer which shows the absence of the charge cloud. The mapping of the ELF surface shown above the ELF surface comprises of rise and fall in the peaks. The rise in the peaks indicates a charge cloud and the depression in the peaks indicates the lack of the charge cloud [48]. There seem raised peaks over the 7DMC and depression in peaks above the Ag₃ trimer. This supports the charge of transportation. Fig. 4 (b) indicates the TDM map of the 7DMC+Ag₃ combination. The red spot in the TDM map indicates the availability of the charge. The red spots were observed for atoms 2O and 17C of the carbonyl group. The interaction between the 7DMC and Ag₃ trimer was also established by the TDM map. The interactive bond 2O-35Ag formed between the trimer and 7DMC in the optimized geometry was supported by the TDM map. Thus, the TDM map suggests the 17C-2O group as the perfect adsorption site for the trimer.

3.5. Natural charge and bond order analysis

The comparison of the charges in water, methanol, and DMF has been shown in Fig. 5. The charge distribution of the 7DMC+Ag₃ combination shows the positive charge contribution of the Ag atoms and the negative charge contribution of oxygen (1O and 2O) and nitrogen (3N) atoms of the 7DMC molecule. The carbon atoms contribute positively as well as negatively to the total charge contribution. The atom 17C attached to the 2O atom in the carbonyl group contributes positively. The variation in the charge of the atoms involved in the intramolecular interactions shows the possibility of intramolecular charge transfer. To support the interpretation presented by the charge distribution, the NBO analysis was also done for the 7DMC+Ag₃ combination in water, methanol, and DMF and has been listed in Table 3. The stabilization energy computed for all the obtained donor-acceptor pairs in the NBO calculations presented that the most stable interaction was found to be between 2O and 35Ag. After the optimization, the bond 2O-35Ag formed between 7DMC and trimer was found most stabilized. The stabilization energy between lone pairs of 2O and 35Ag was found highest at 7.92, 7.58, and 7.46 kcal/mol. Even the other interactions were found between the trimer and C=O carbonyl group. Thus, the NBO analysis and the charge transfer validated the intermolecular interactions between the trimer and 7DMC molecule.

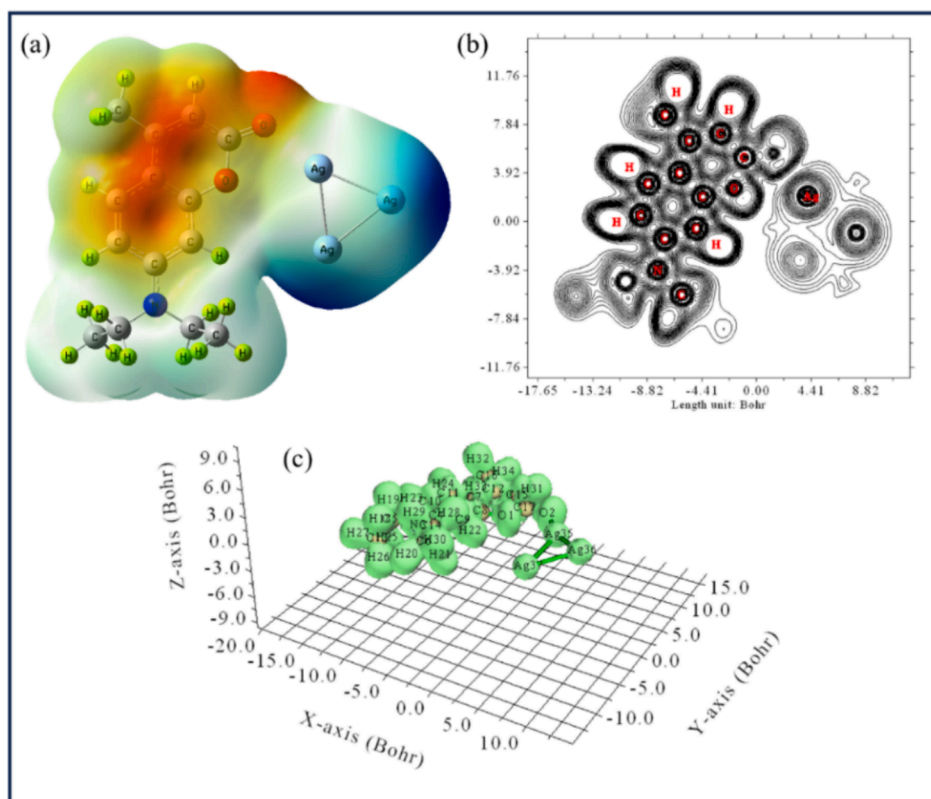


Fig. 3. (a) MEP surface, (b) counterplots of 7DMC+Ag₃ combination, (c) molecular isosurface of 7DMC+Ag₃ combination.

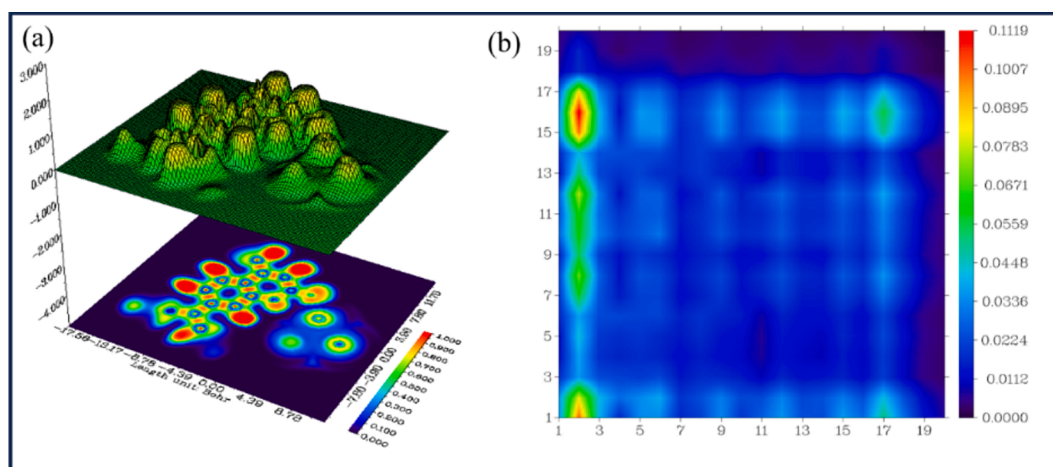


Fig. 4. (a) ELF surface, and (b) TDM plot of 7DMC+Ag₃ combination.

3.6. Inter-fragment charge transfer analysis

The results obtained from the IFCT analysis done for the 7DMC+Ag₃ combination have been tabulated in Table 4 and the net charge transferred from silver trimer towards the carbonyl group of 7DMC has been illustrated in Fig. 6. The molecule 7DMC has higher hole and electron concentrations as compared to the Ag₃ trimer. The total transferred charge from fragment 1 (7DMC) to fragment 2 (Ag₃ trimer) was lower and the total transferred charge from fragment 2 towards fragment 1 was higher. This was in great agreement with the results obtained from molecular surfaces and NBO analysis. This justifies the donor nature of the Ag₃ trimer and the acceptor nature of the 7DMC molecule. The net transferred charge in the 7DMC+Ag₃ combination in water, methanol, and DMF were $-0.02 e$, $-0.01 e$, and $-0.01 e$ respectively. The values of

intrinsic as well as apparent local excitation were higher than the values of intrinsic and apparent charge transfer. Thus, the IFCT analysis suggests the occurrence of local excitation of charge from Ag₃ to 7DMC. Moreover, this confirms the strong stability of the 7DMC+Ag₃ combination.

3.7. Electronic properties

The computed absorption spectra of the 7DMC+Ag₃ combination in water, methanol, and DMF are illustrated in SD 1 and the obtained electronic transition is listed in SD 2. As mentioned in the previously published article on the NLO activity of probe 7DMC molecule, the experimental absorption spectra of 7DMC were observed between 300 to 450 nm with the highest peak at 370 nm wavelength. The simulated

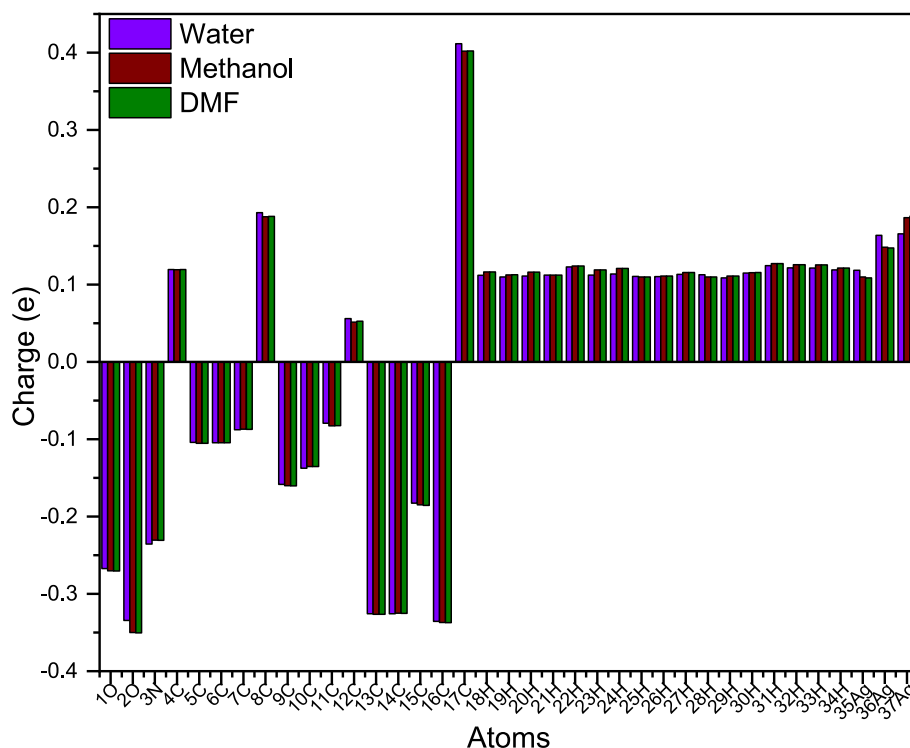


Fig. 5. Natural charge of 7DMC+Ag₃ combination in water, methanol, and DMF.

Table 3

Second-order perturbation theory analysis of Fock Matrix in NBO basis of 7DMC and 7DMC+Ag₃ combination (LP- lone pair, LP*- anti-bond lone pair, BD- bonding orbital, BD*-antibonding orbital, CR-one core pair).

S. no.	Donor NBO (i)	Acceptor NBO (j)	E(2) (kcal/mol)	E(j)-E(i) (au)	F(i, j) (au)
Between 7DMC and Ag₃					
Water					
1.	LP (1) 2O	LP* (6) 35Ag	7.92	0.83	0.1
2.	LP (2) 2O	LP* (6) 35Ag	4.51	0.50	0.06
3.	LP (2) 2O	BD* (1) 35Ag-36Ag	1.06	0.49	0.02
4.	LP (1) 1O	LP* (6) 35Ag	0.68	0.72	0.02
5.	CR (1) 35Ag	BD* (1) 2O-17C	0.41	4.02	0.05
Methanol					
1.	LP (1) 2O	LP* (6) 35Ag	7.58	0.84	0.1
2.	LP (2) 2O	LP* (6) 35Ag	3.86	0.51	0.05
3.	LP (2) 2O	BD* (1) 35Ag-36Ag	1.70	0.51	0.03
4.	LP (1) 1O	LP* (8) 37Ag	0.16	0.63	0.01
5.	CR (1) 35Ag	BD* (1) 2O-17C	0.35	4.00	0.04
DMF					
1.	LP (1) 2O	LP* (6) 35Ag	7.46	0.84	0.1
2.	LP (2) 2O	LP* (6) 35Ag	3.85	0.50	0.05
3.	LP (2) 2O	BD* (1) 35Ag-36Ag	1.65	0.51	0.03
4.	LP (1) 1O	LP* (8) 37Ag	0.17	0.62	0.01
5.	CR (1) 35Ag	BD* (1) 2O-17C	0.33	4.00	0.04

absorption peak was observed at 341 nm. The transitions of the experimental range were observed as $\pi-\pi^*$ [47,48]. After the introduction of the Ag₃ trimer, there was a bathochromic shift in the absorption peak of the 7DMC+Ag₃ combination. The absorption spectra of the 7DMC+Ag₃ combination were observed between the visible ranges of 300–700 nm for all the solvents. However, the peak of the spectra in water, methanol,

Table 4

Results from the IFCT analysis for 7DMC+Ag₃ combination in water, methanol, and DMF [IFER-Intra-fragment electron redistribution, IFCT (electrons)-magnitude of the transferred charge, IFCT (%) - percentage of the transferred charge, CT(I)-intrinsic charge transfer percentage, LE(I)-intrinsic local excitation percentage, CT(A)-apparent charge transfer percentage, LE(A)-apparent local excitation percentage].

Properties		Water	Methanol	DMF
Fragment-1 (7DMC)	Hole (%)	97.24	97.61	97.63
	Electron (%)	99.53	99.58	99.50
Fragment-2 (Ag ₃)	Hole (%)	2.76	2.39	2.37
	Electron (%)	0.47	0.42	0.50
IFER	IFER (1)	0.96	0.97	0.97
	IFER (2)	0.00013	0.00010	0.00012
IFCT (electrons)	1 → 2	0.0046	0.00412	0.0049
	2 → 1	0.02	0.02	0.02
	Net charge	-0.02	-0.01	-0.01
IFCT (%)	CT (I)	3.2	2.79	2.85
	LE (I)	96.79	97.2	97.14
	CT (A)	2.29	1.96	1.87
	LE (A)	97.71	98.03	98.12

and DMF was observed at 516, 531, and 529 nm with excitation energy 2.4, 2.33, and 2.34 eV respectively. The observed range of the absorption shows the $n-\pi^*$ nature of the transitions for the 7DMC+Ag₃ combination [49]. Moreover, the shifting of the HOMO-LUMO surfaces also supports the excitation of the charges in the molecular orbitals. The green and red colored surfaces shown in Fig. 7 show the negative and positive nature of the molecular orbital wave function, respectively. The HOMO-LUMO surfaces were shifted from the Ag₃ trimer over the complete geometry of 7DMC. Therefore, the interpretation imaged by MEP surface and NBO analysis that trimer acts as donor and 7DMC acts as acceptor groups. Thus, high chemical reactivity and intramolecular charge transfer were the outcome and verified by the electronic transitions and HOMO-LUMO surfaces.

Fig. 8 illustrates the theoretical and experimental absorption spectra of 7DMC+Ag₃ and 7DMC+AgNps respectively. A broad theoretical

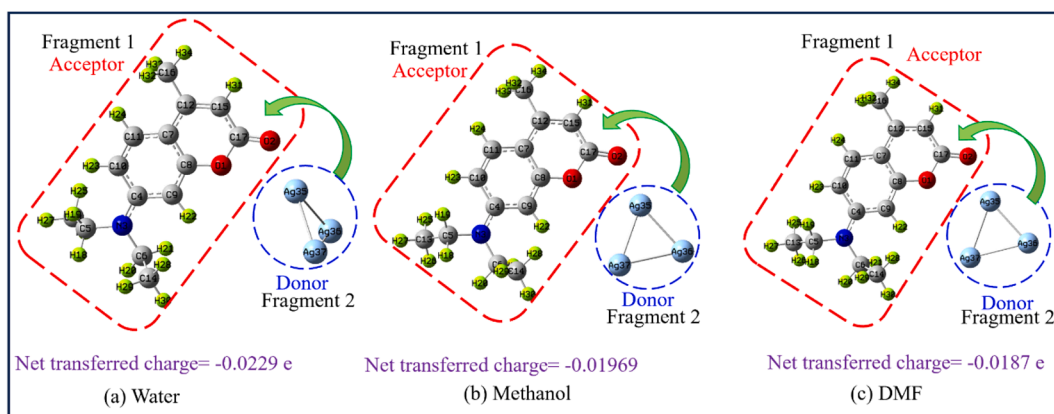


Fig. 6. Inter fragment charge transfer shows the nature of charge transfer from the donor candidates towards the acceptor candidates in the 7DMC+Ag₃ combination.

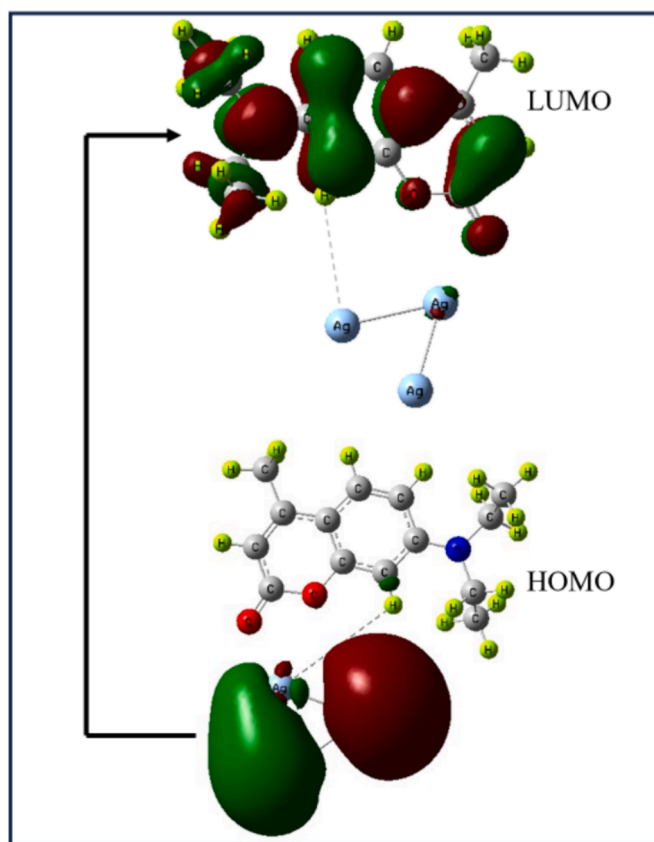


Fig. 7. HOMO-LUMO surface distribution of 7DMC+Ag₃ trimer.

absorption band of 7DMC+Ag₃ was observed in the wavelength range of 350 to 700 nm. The crucial transition of the 7DMC+Ag₃ was observed at 449 nm with oscillator strength of 0.04. The theoretical absorption band of probe 7DMC was observed in range 250 and 450 nm [34]. The comparison of the 7DMC+Ag₃ and probe 7DMC indicated that the absorption band of 7DMC was shifted from 250–450 nm to 350–700 nm range showing the bathochromic shift. As discussed earlier, the shift was due to the introduction of Ag₃ trimer. The occurrence of red shift in absorption spectra also supported the adsorption between the 7DMC and AgNps due to electrostatic interactions between both the candidates. The experimental absorption spectra of 7DMC+AgNps was in wavelength range 300 and 700 nm which was in good agreement with the theoretical absorption spectra. The experimental absorption peak of the 7DMC+AgNps was observed at around 400 nm. The comparison of the

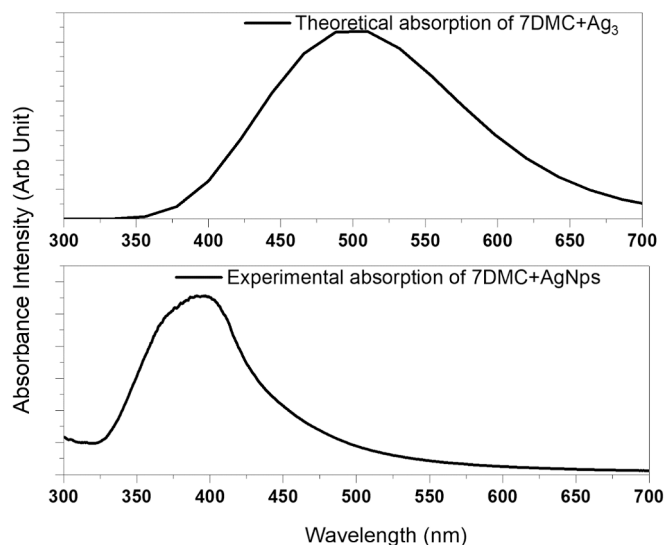


Fig. 8. Theoretical absorption spectra of PABA+Ag₃ and experimental absorption spectra of 7DMC+AgNps.

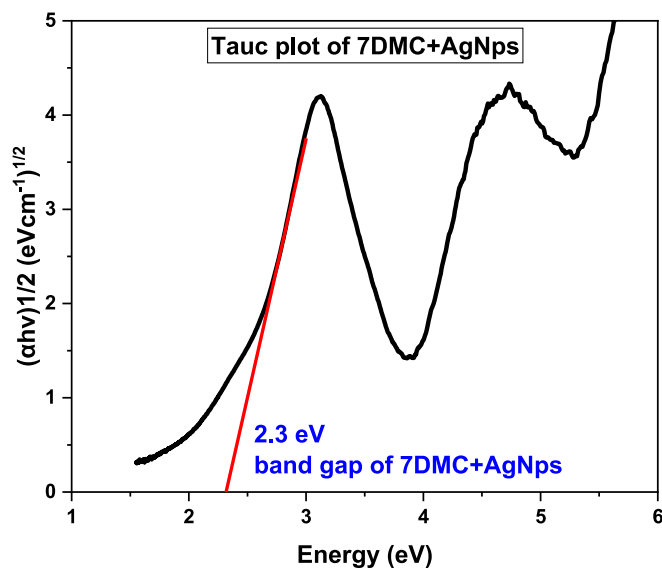


Fig. 9. Tauc plot of 7DMC+AgNps.

theoretical and experimental absorption bands in both the cases indicated that the results are in accord to each other. Fig. 9 indicated the Tauc plot for 7DMC+AgNps. The value of the experimental band gap was observed at 2.3 eV for 7DMC+AgNps. The band gap of 7DMC+AgNps was reduced from the band gap values of probe 7DMC (3.7 eV). After the addition of AgNps, the band gap of 7DMC+AgNps was obtained as 2.3 eV. The reduction in the band gap of 7DMC+AgNps indicated their increased chemical reactivity. The rise in the chemical reactivity supported the occurrence of the strong electronic transitions.

3.8. Vibrational properties

The vibrational modes of the 7DMC+Ag₃ combination in water, methanol, and DMF were obtained and plotted. SD 3 shows the labeled FT-IR spectra of the 7DMC+Ag₃ combination in the considered solvents. The major FT-IR peaks were obtained between 1000–1800 cm⁻¹. The torsional bending (δ), rocking (ρ), and linear symmetric stretching (ν) were the major modes that were obtained for the 7DMC+Ag₃ combination. A sharp peak of δ_{CH} mode was obtained at 1179 cm⁻¹ in all the solvents. The 5C-3 N and 6C-3N bonds were observed to give rocking mode at 1242 cm⁻¹ in water and 1236 cm⁻¹ in methanol and DMF. The $\delta_{\text{C-N}}$ mode had two strong peaks at 1305 and 1399 cm⁻¹ in water, 1305 and 1393 cm⁻¹ in methanol, and 1304 and 1392 cm⁻¹ in DMF. The bond 3 N=4C was observed to give a strong peak at 1468 cm⁻¹ in water. Corresponding to this, $\delta_{\text{C=N}}$ mode at 1467 cm⁻¹ was observed in methanol and DMF. The same bond got stretched at 1579, 1573, and 1572 cm⁻¹ in water, methanol, and DMF. The 17C=2O bond of the carbonyl group gave $\nu_{\text{C=O}}$ mode at 1617, 1607, and 1606 cm⁻¹ in water, methanol, and DMF. The C=C bonds of the benzene ring vibrate linearly and give strong peaks at 1634 and 1695 cm⁻¹ in water. In methanol, the peak was not prominent but was significant at 1634 and 1696 cm⁻¹. In DMF, the $\nu_{\text{C=C}}$ mode was observed at 1621 and 1694 cm⁻¹. The theoretical vibrational spectra of 7DMC+Ag₃ combination in methanol was further compared with the experimental FT-IR spectra of 7DMC+AgNps (Fig. 10). The active functional groups in 7DMC gave significant responses to the infrared radiation showing the higher ability of polarization of the 7DMC+Ag₃ combination. Moreover, the higher value of infrared activity for the combination shows a higher probability of the NLO responses of the 7DMC+Ag₃ combination. The major experimental FT-IR peaks were obtained between 1000–1800 cm⁻¹. The bending of C-H was observed at 1100 cm⁻¹ in theoretical and 1043 cm⁻¹ in experimental FT-IR spectra. In probe 7DMC, this mode was noticed in 1392 cm⁻¹. The stretching of C=C bonds gave peaks in theoretical FT-IR

spectra at 1620 and 1700 cm⁻¹. These peaks were corresponding to the 1637 cm⁻¹ peak in experimental spectra. The N-H modes were obtained at high intensity at 3068 and 3172 cm⁻¹. To the contrary, the experimental FT-IR band was obtained near 3308 cm⁻¹ for stretching of the N-H bonds. The FT-IR for 7DMC+Ag₃ and 7DMC+AgNps were also in good agreement in each other. The theoretical and experimental FT-IR spectra coincide each other and validated that the major modes were corresponding to the available functional groups. The peak for $\nu_{\text{C=C}}$ observed at 1637 cm⁻¹ in experimental FT-IR spectra corresponded to the peak observed for the same vibrational mode in FT-IR spectra of probe 7DMC at 1658 cm⁻¹ [34]. There was a downshift in the vibrational modes of the 7DMC+AgNps as compared to the probe 7DMC. This downshift in IR intensity confirmed the occurrence of electrostatic interactions between 7DMC and AgNps. Moreover, the addition of AgNps resulted in the increased chemical reactivity and enhanced NLO activity of the 7DMC+AgNps.

3.9. Polarizability and hyperpolarizability analysis

The μ_{total} is the total extent of the polarization of the system [50]. From the results, it was observed that the value of μ_{total} increases for combination water but was reduced for methanol and DMF. This might be due to the polar nature of the solvent water as compared to methanol and DMF. The polarizability parameters α_{total} and $\Delta\alpha$ denote the isotropic and anisotropic polarizability of the 7DMC+Ag₃ combination. The α_{total} is a measure of the uniform properties of the combination throughout the geometry and is mostly higher for the centrosymmetric bodies whereas the $\Delta\alpha$ denotes the nonuniformity of the properties in the molecules and is mostly higher for non-centrosymmetric structures [51] (Table 5). This can also be interpreted as the compounds with higher α_{total} show linear opticality and compounds with higher $\Delta\alpha$ denote optical nonlinearity. The 7DMC+Ag₃ combination has an increasing value of α_{total} as water < methanol < DMF. This shows that the 7DMC+Ag₃ combination shows linear behavior higher in DMF and lower in water. The value of $\Delta\alpha$ is the measure of the optical nonlinearity of the molecule. The value of the 7DMC+Ag₃ combination was high as compared to that of the probe 7DMC. The value of $\Delta\alpha$ of 7DMC+Ag₃ combination was in increasing order as water < DMF < methanol. This interpreted the higher optical nonlinearity of the 7DMC+Ag₃ combination in water. The expansion of the polarization in the availability of a higher electric field (in the case of the NLO effect) leads to the violation of the superposition principle and it results in the splitting of the coefficient of electric field in increasing orders such as β, γ, \dots [50]. The higher value of these coefficients validated the NLO effect of the target molecule. In other words, theoretically, we can prove that the molecules exhibiting higher values of these NLO coefficients possess the NLO effect. The 7DMC+Ag₃ combination has the highest value of β_{total} in water (2002.71×10^{-30} esu), followed by methanol (778.72×10^{-30} esu), and then DMF (677.12×10^{-30} esu). The values reveal that the 7DMC+Ag₃ combination shows the highest NLO activity in water. The value of the β_{total} of 7DMC+Ag₃ combination was higher as compared to that of probe 7DMC. This also validates the increment in the NLO behavior of the 7DMC after the adsorption of the Ag₃ trimer. Table 6 lists the values of the β_{total} of some silver trimer adsorbed systems. The comparison

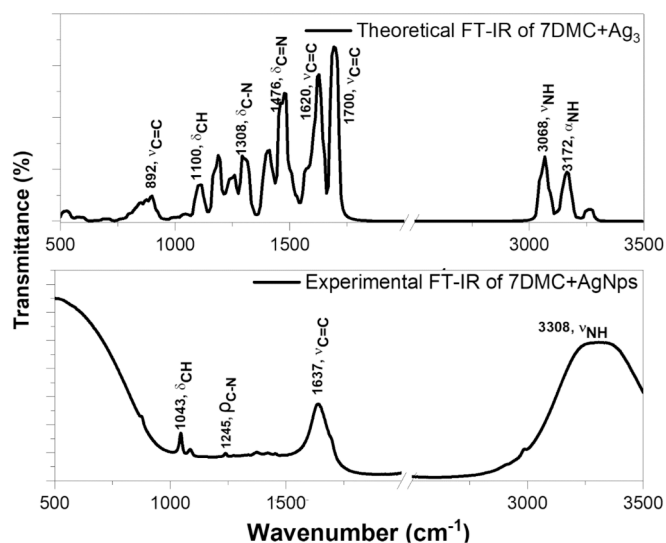


Fig. 10. FT-IR spectra of 7DMC+Ag₃ and 7DMC+AgNps.

Table 5
Comparison of the NLO parameters of probe 7DMC and 7DMC+Ag₃ combination in water, methanol, and DMF.

Properties	7DMC	7DMC Ag ₃ (Water)	7DMC+Ag ₃ (Methanol)	7DMC+Ag ₃ (DMF)
μ_{total}	11.12	12.03	4.99	4.95
α_{total}	27.22×10^{-24}	77×10^{-24}	97.57×10^{-24}	99.45×10^{-24}
$\Delta\alpha$	75.92×10^{-24}	221.82×10^{-24}	239.67×10^{-24}	233.21×10^{-24}
β_{total}	18.46×10^{-30}	2002.71×10^{-30}	778.72×10^{-30}	677.12×10^{-30}

Table 6

Comparison of the β_{total} of 7DMC+Ag₃ with other reference studies (values are in esu).

Properties	β_{total}	Reference
7DMC+Ag ₃	2002.71×10^{-30}	–
QA+Ag ₃	930×10^{-30}	[22]
2,9-DMQA+Ag ₃	1163×10^{-30}	[23]
Chr-Ag ₃	261×10^{-30}	[24]
TeH-Ag ₃	331×10^{-30}	[24]
TeP-Ag ₃	432×10^{-30}	[24]
TrP-Ag ₃	206×10^{-30}	[24]
Py-Ag ₃	435×10^{-30}	[24]
PD-Ag ₃	184.22×10^{-30}	[26]
Nitropyrene + Ag ₃	2071.63×10^{-30}	[27]
PABA+Ag ₃	127.59×10^{-30}	[28]

shows that the value of β_{total} of 7DMC+Ag₃ was higher than all of the referred combination.

3.10. Nonlinear optical and laser limiting responses

The Nd:YAG laser was used to perform the Z-Scan experiment. In this experiment, the synthesized liquid samples of AgNps and 7DMC+AgNps was excited with a focused laser beam. The normalized transmittance as a function of position along the direction of propagation of beam i.e., Z (mm) was measured and is defined as Z-Scan pattern. Mechanically, a stepper motor is used in Z-Scan instrument and the sample is moved along the negative as well as positive direction [51]. Corresponding to each step, the value of normalized transmittance at that specific position is taken as a data plot. After the calculations of all the data points, the data fitting is done. Two different configurations of the Z-scan experiment are possible i.e., a peak or a valley at the focus. The former shows occurrence of Saturable Absorption (SA) and latter indicate Reverse Saturable Absorption (RSA) [51]. The RSA is the measure of the decrement in the transmittance of the sample with the increase in excitation laser power. The open-aperture Z-Scan analysis was performed for the AgNps and 7DMC+AgNps at the pulse energy of 100 μJ . The NLO and OL pattern of the prepared AgNps was shown in the Fig. 11. In the Z-Scan pattern of AgNps, a valley-shaped curve symmetric about the focus (Z=0) axes was obtained and the valley represent the occurrence of the RSA in synthesized AgNps. The best fit solid line obtained from the experimental data (scattered points) indicate the occurrence of the RSA. The OL pattern of the AgNps indicated the linear behavior of the normalized transmittance with the input fluence but with further increment in the input fluence, the normalized transmittance starts deviating towards the origin. Thus, at low intensities, the normalized transmittance was not altered by the input fluence but after

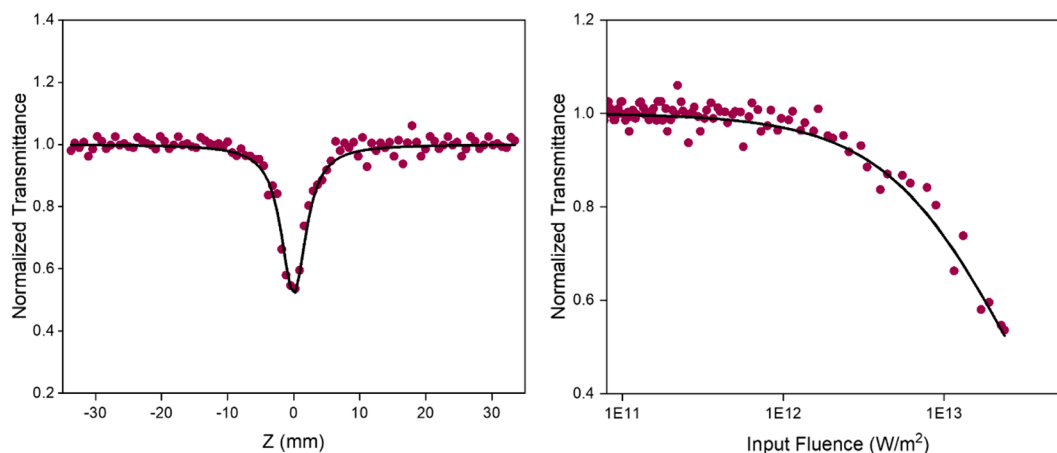


Fig. 11. Z-Scan and optical limiting pattern of AgNps.

reaching a certain cut off, it shows nonlinear pattern.

Similar kind of patterns in the Z-Scan and OL was observed for the 7DMC+AgNps. The open-aperture Z-Scan experiment of the 7DMC+AgNps (Fig. 12) shows that it also exhibits nonlinear absorption. The valley-like pattern with the maximum intensity at the focus indicates the occurrence of the RSA in the 7DMC+AgNps. The inset of Fig. 12 illustrates the Z-Scan curve of the probe 7DMC. The comparison of the Z-Scan pattern of the 7DMC+AgNps and probe 7DMC indicated that the data points in case of 7DMC+AgNps were more likely to be observed near the fitting line as compared to that in the case of probe 7DMC. This indicates the enhanced NLO activity of the 7DMC+AgNps as compared to that of probe 7DMC. This was also supported by the decrement in the nonlinear absorption coefficient values of 7DMC+AgNps (0.6×10^{-10} m/W) from the value of same for probe 7DMC (0.65×10^{-10} m/W) (Table 7). The OL pattern plotted for 7DMC+AgNps (Fig. 13) also gave a decrement in the normalized transmittance of the sample with the increase in the input fluence. The inset of Fig. 13 indicates the OL graph of probe 7DMC. It is already known that the 7DMC has NLO and OL characteristics [29]. The OL threshold of 7DMC of probe 7DMC was reported as 2.67×10^{13} W/m² and that of 7DMC+AgNps was observed as 2.15×10^{13} W/m². The decrement in the optical limiting threshold of 7DMC+AgNps indicates

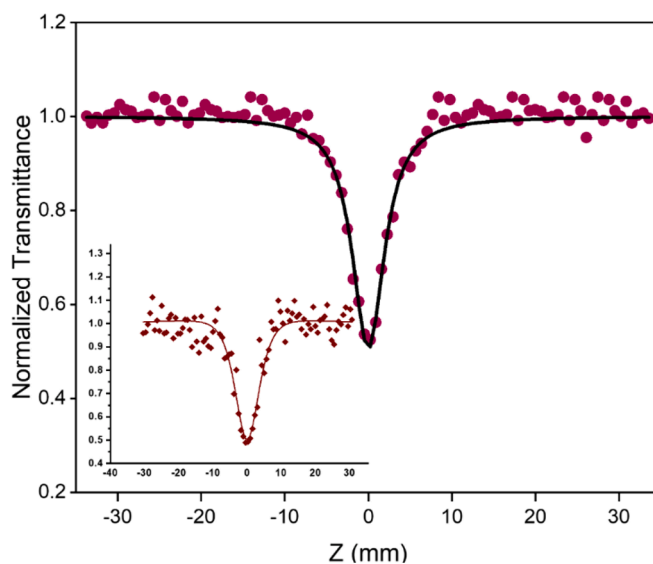


Fig. 12. Z-Scan pattern of 7DMC+AgNps. Inset of the graph indicates the Z-Scan pattern of probe 7DMC [29].

Table 7

Saturation intensity, nonlinear absorption coefficient, and optical limiting threshold of 7DMC [29], AgNps, and 7DMC+AgNps.

Compounds	7DMC	AgNps	7DMC+AgNps
Saturation Intensity ($\times 10^{12}$ W/m ²)	40	20	20
Nonlinear Absorption Coefficient ($\times 10^{-10}$ m/W)	0.65	0.58	0.60
Optical Limiting Threshold ($\times 10^{13}$ W/m ²)	2.67	2.33	2.15

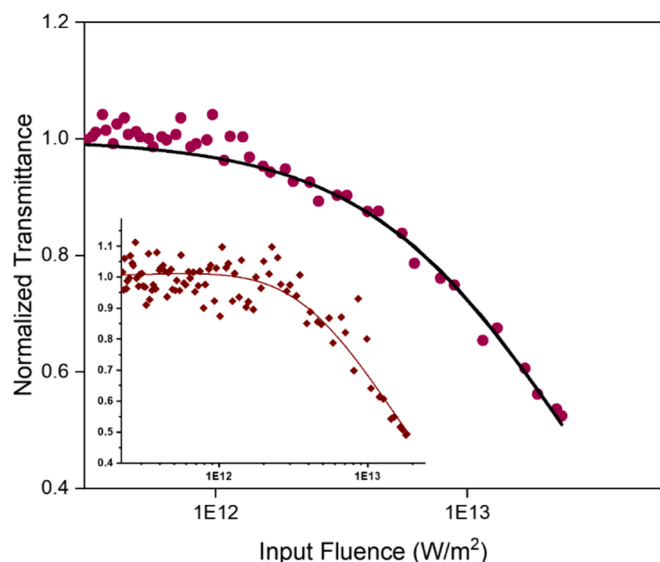


Fig. 13. Optical limiting pattern of 7DMC+AgNps. Inset of the graph indicates the optical limiting pattern of probe 7DMC [29].

the occurrence of strong two-photon absorption in 7DMC+AgNps as compared to 7DMC. Therefore, the NLO and OL responses reported in the present study suggests strong potentiality of 7DMC+AgNps to be used for the fabrication of the laser protection devices.

4. Conclusion

Nanomaterials have reported outstandingly large optical nonlinearity. Previously, we have done optical limiting characteristics of 7DMC. Herein, we have reported the NLO activity of the 7DMC combined with AgNps via computational and experimental analysis. Various charged surfaces like MEP surface, molecular orbitals surfaces, counterplots, and molecular isosurface successfully established the path of intramolecular charge transfer from Ag₃ trimer towards 7DMC. The TDM plot and ELF surfaces confirm the localization of the charge cloud over the 17C-2O group of 7DMC. The IFCT analysis helped in identifying the exact quantity of the charge transferred from trimer (-0.02 e, -0.01 e, and -0.01 e) to 7DMC in water, methanol, and DMF respectively. The absorption spectra of the 7DMC+Ag₃ combination were shifted to 300–700 nm as compared to the absorption spectra of probe 7DMC (300–450 nm). The theoretical and experimental absorption spectra were in good agreement with each other. The vibrational spectra were capable of showing the higher responsive peaks of the available functional group towards the infrared radiation. It was also observed that the vibrational modes of 7DMC+AgNps were downshifted as compared to that for the probe 7DMC. The NLO property was finally established by the value of β_{total} . The value of β_{total} was higher for water (2002.71×10^{-30} esu). The valley-like shape observed in the Z-Scan spectra finally justified the NLO responses of 7DMC+AgNps. It also supported the occurrence of the RSA in the combined samples. The OL spectra gave a decrement in the normalized transmittance with the increase in the input fluence. Thus, the OL spectra clearly states that the proposed

liquid sample can be used as an optical limiter. Further, the proposed study can be a basis for the further fabrication of the laser safety devices using 7DMC+AgNps.

Ethical approval

This material is the author's original work, which has not been previously published elsewhere. All authors have been personally and actively involved in substantial work leading to the paper and will take public responsibility for its content. The paper properly credits the meaningful contributions of all the co-authors.

Funding

S. Lakhera and M. Rana thank Uttarakhand Science Education and Research Centre (USERC), Department of Information and Science Technology, Government of Uttarakhand, for financial support through an R&D Research Project (Project no: USERC/2023-24/190).

CRediT authorship contribution statement

Shradha Lakhera: Writing – original draft, Visualization, Validation, Software, Investigation, Data curation. **Meenakshi Rana:** Writing – review & editing, Validation, Supervision, Methodology, Conceptualization. **Vivek Dhuliya:** Writing – original draft, Software, Investigation. **L.P. Purohit:** Visualization, Supervision, Resources. **A. Dhanusha:** Project administration, Data curation. **T.C. Sabari Girisun:** Resources, Methodology.

Declaration of competing interest

The authors declare that they have no known competing financial interests or personal relationships that could have appeared to influence the work reported in this paper.

Data availability

All data generated or analyzed during this study, which support the plots within this paper and the other findings of this study, are included in this article and its [Supplementary Information](#). Source data are provided in this paper.

Appendix A. Supplementary data

Supplementary data to this article can be found online at <https://doi.org/10.1016/j.jphotochem.2024.115910>.

References

- [1] S. Jeyaram, Spectral, third-order nonlinear optical and optical switching behavior of β -carotenoid extracted from phyllanthus niruri, Indian J. Phys. 96 (2022) 1655–1661, <https://doi.org/10.1007/s12648-021-02122-0>.
- [2] S.J. Sharma, K.K. Sonigara, H.K. Machhi, S.S. Soni, N. Sekar, Significance of anchoring group design on light harvesting efficiency of dye-sensitized solar cells and non-linear optical response, J. Mol. Struct. 1294 (1) (2023) 136435, <https://doi.org/10.1016/j.molstruc.2023.136435>.
- [3] M. Rana, N. Singla, A. Chatterjee, A. Shukla, P. Chowdhury, Investigation of nonlinear optical (NLO) properties by charge transfer contributions of amine-functionalized tetraphenylethylene, Opt. Mater. 62 (2016) 80–89, <https://doi.org/10.1016/j.optmat.2016.09.043>.
- [4] P. Yadav, M. Rana, P. Chowdhury, DFT and MD simulation investigation of favipiravir as an emerging antiviral option against viral protease (3CLpro) of SARS-CoV-2, J. Mol. Struct. 1246 (2021) 131253, <https://doi.org/10.1016/j.molstruc.2021.131253>.
- [5] L. Wen, L. Zhou, B. Zhang, M. Bingguang, X. Meng, H. Qu, D. Hua, D. Li, Multifunctional amino-decorated metal-organic frameworks: nonlinear-optic, ferroelectric, fluorescence sensing and photocatalytic properties, J. Mater. Chem. 22 (42) (2012) 22603, <https://doi.org/10.1039/c2jm34349e>.
- [6] A. Ramalingam, M. Kuppusamy, S. Sambandam, M. Medimagh, O. E. Oyenyin, A. Shanmugasundaram, N. Issaoui, N. D. Ojo, N. D., Synthesis, spectroscopic, topological, hirshfeld surface analysis, and anti-covid-19 molecular docking

- investigation of isopropyl 1-benzoyl-4-(benzoyloxy)-2,6-diphenyl-1,2,5,6-tetrahydropyridine-3-carboxylate. *Heliyon*. 8 (10) (2022) E 10831. doi: 10.1016/j.heliyon.2022.e10831.
- [7] S. Lakhera, M. Rana, K. Devlal, Investigation of Nonlinear Optical Responses of Organic Derivative of Imidazole: Imidazole-2-carboxaldehyde, *IJMR*. 114 (7–8) (2023) 555–563, <https://doi.org/10.1515/ijmr-2021-8649>.
- [8] G. Deng, H. Xu, L. Kuang, C. He, B. Li, M. Yang, X. Zhang, Z. Li, J. Liu, Novel nonlinear optical chromophores based on coumarin: Synthesis and properties studies, *Opt. Mater.* 88 (2019) 218–222, <https://doi.org/10.1016/j.optmat.2018.11.035>.
- [9] J. Suryapratap, Sharma, Nagaiyan Sekar, Deep-red/NIR emitting coumarin derivatives - Synthesis, photophysical properties, and biological applications, *Dyes Pigm.* 202 (2022) 110306, <https://doi.org/10.1016/j.dyepig.2022.110306>.
- [10] N. Pandey, M.S. Mehata, S. Pant, et al., Structural, Electronic and NLO Properties of 6-aminoquinoline: A DFT/TD-DFT Study, *J Fluoresc.* 31 (2021) 1719–1729, <https://doi.org/10.1007/s10895-021-02788-z>.
- [11] M. Rana, A. Chatterjee, P. Chowdhury, Investigation of nonlinear optical properties of organic-based di amine substituted tetraphenylethylene AIP Conf, Proc. 2009 (2018) 020055, <https://doi.org/10.1063/1.5052124>.
- [12] S. Lakhera, K. Devlal, M. Rana, V. Dhuliya, Quantum Mechanical Study of Three Aromatic Bioactive Fatty Alcohol Compounds with Nonlinear Optical and Potential Light Harvesting Properties, *Opt. Mater.* 129 (2022) 112476, <https://doi.org/10.1016/j.optmat.2022.112476>.
- [13] S. Lakhera, M. Rana, K. Devlal, Theoretical study on spectral and optical properties of essential amino acids: a comparative study, *Opt Quantum Electron.* 54 (2022) 714, <https://doi.org/10.1007/s11082-022-04118-4>.
- [14] S. Lakhera, K. Devlal, M. Rana, I. Celik, Study of nonlinear optical responses of phytochemicals of *Clitoria ternatea* by quantum mechanical approach and investigation of their anti-Alzheimer activity with in silico approach, *Struct Chem* (2022), <https://doi.org/10.1007/s11224-022-01981-5>.
- [15] M. Rana, P. Yadav, P. Chowdhury, DFT investigation of the nonlinear optical response of organic compound: acetylsalicylic acid, *IJMR*. 114 (7–8) (2023) 527–535, <https://doi.org/10.1515/ijmr-2021-8732>.
- [16] P. N. Prasad, D. J. Williams, Introduction to nonlinear optical effects. In *Molecules and Polymers*, Wiley, New York (1991).
- [17] S. Lakhera, K. Devlal, M. Rana, Investigation of the electronic and optical activity of halogen-substituted 2-nitrotoluene by density functional theory, *Opt Quant Electron* 55 (2023) 292, <https://doi.org/10.1007/s11082-023-04569-3>.
- [18] S. Lakhera, K. Devlal, M. Rana, V. Dhuliya, Computational study of non-linear optical and electrical properties of 1,3-dinitropyrene, *Opt Quant Electron* 55 (2023) 85, <https://doi.org/10.1007/s11082-022-04371-7>.
- [19] M. Rana, P. Chowdhury, Perturbation of hydrogen bonding in hydrated pyrrole-2-carboxaldehyde combinations, *J Mol Model* 23 (2017) 216, <https://doi.org/10.1007/s00894-017-3380-2>.
- [20] C.A. Njeumen, G.W. Ejuh, Y.T. Assatse, R.A.Y. Kamsi, J.M.B. Ndjaka, DFT studies of physico-chemical, electronic and nonlinear optical properties of interaction between doped-fullerenes with non-steroidal anti-inflammatory drugs, *Phys. B Condens. Matter* 665 (2023) 415041, <https://doi.org/10.1016/j.physb.2023.415041>.
- [21] S. Renuga, S. Muthu, Molecular structure, normal coordinate analysis, harmonic vibrational frequencies, NBO, HOMO–LUMO analysis and detonation properties of (S)-2-(2-oxopyrrolidin-1-yl) butanamide by density functional methods, *Spectrochim Acta A Mol Biomol Spectrosc.* 118 (2014) 702–715, <https://doi.org/10.1016/j.saa.2013.09.055>.
- [22] E. Elamurugu Porchelvi, S. Muthu, Vibrational spectra, molecular structure, natural bond orbital, first order hyperpolarizability, thermodynamic analysis and normal coordinate analysis of Salicylaldehyde p-methylphenylthiosemicarbazone by density functional method, *Spectrochim Acta A Mol Biomol Spectrosc.* 134 (2015) 453–464, <https://doi.org/10.1016/j.saa.2014.06.018>.
- [23] B. Amul, S. Muthu, M. Raja, S. Sevvanthi, Spectral, DFT and molecular docking investigations on Etodolac, *J. Mol. Struct.* 1195 (2019) 747–761, <https://doi.org/10.1016/j.molstruc.2019.06.047>.
- [24] Suryapratap J. Sharma, Jyoti Prasad, Saurabh S. Soni, Nagaiyan Sekar, The impact of anchoring groups on the efficiency of dye-sensitized solar cells: 2-Cyanoacrylic acid vs. ethyl 2-cyanoacrylate, *J. Photochem. Photobiol. A*. 444 (2023) 114915. doi: 10.1016/j.jphotochem.2023.114915.
- [25] P. Sankar, R. Philip, S.M. Bhagyaraj, O.S. Oluwafemi, N. Kalarikkal, S. Thomas, Chapter 11 - Nonlinear Optical Properties of Nanomaterials, in: *Micro and Nano Technologies, Characterization of Nanomaterials*, Woodhead Publishing, 2018, pp. 301–334, <https://doi.org/10.1016/B978-0-08-101973-3.00011-0>.
- [26] S. Knoppe, H. Häkkinen, T. J. Verbiest, Nonlinear Optical Properties of Thiolate-Protected Gold Clusters: A Theoretical Survey of the First Hyperpolarizabilities *Phys. Chem. C*. doi: 10.1021/acs.jpcc.5b08341.
- [27] U.R. Felscia, B.J.M. Rajkumar, Computational study of quinaclidone on silver and gold clusters: applications to organic light emitting diodes and nonlinear optical devices, *Mater. Lett.* (2018), <https://doi.org/10.1016/j.matlet.2018.03.149>.
- [28] S. Lakhera, K. Devlal, M. Rana, V. Dhuliya, N. Pandey, Non-Linear Optical Behavior of 2,9-Dimethylquinacridone with Adsorbed Gold and Silver Nanoclusters, *Optik* 170983 (2023), <https://doi.org/10.1016/j.joee.2023.170983>.
- [29] U.R. Felscia, B.J.M. Rajkumar, M.B. Mary, Theoretical investigations on nonlinear fused 4-ring systems: Application to OLED and NLO devices, *Synth. Met.* 246 (2018) 31–38, <https://doi.org/10.1016/j.synthmet.2018.09.008>.
- [30] Y. Chang, W. Li, Y. Jiang, Effect of separation on second-order hyperpolarizability of two silver nanoclusters, *Phys. Lett. A* 376 (34) (2012) 2314–2318, <https://doi.org/10.1016/j.physleta.2012.05.047>.
- [31] S. Lakhera, M. Rana, K. Devlal, Influence of Adsorption of Gold and Silver Nanoclusters on Structural, Electronic, and Nonlinear optical properties of Pentacene-5, 12-dione: A DFT study, *Opt Quant Electron* 55 (2023) 178, <https://doi.org/10.1007/s11082-022-04422-z>.
- [32] U.R. Felscia, B.J.M. Rajkumar, P. Sankar, R. Philip, M.B. Mary, Theoretical and experimental investigations of nitropyrene on silver for nonlinear optical and metal ion sensing applications, *Mater. Chem. Phys.* (2019), <https://doi.org/10.1016/j.matchemphys.2019.122466>.
- [33] S. Lakhera, K. Devlal, M. Rana, Nonlinear optical response of Silver trimer adsorbed para-aminobenzoic Acid: A DFT study, *Physica Scripta*. doi: 10.1088/1402-4896/ad0084.
- [34] S. Lakhera, K. Devlal, M. Rana, N. Kanagathara, A. Dhanusha, T.C. Sabari Girisun, S. Sharma, P. Chowdhury, Two-photon absorption and optical limiting in 7-diethylamino-4-methyl coumarin, *J. Photochem. Photobiol. A: Chem.* 115216 (2023), <https://doi.org/10.1016/j.jphotochem.2023.115216>.
- [35] M.J. Frisch, Gaussian 09, Revision B.01, Gaussian Inc., Wallingford CT, 2010.
- [36] GaussView, Version 6, Dennington, Roy; Keith, Todd A.; Millam, John M. Semichem Inc., Shawnee Mission, KS (2016).
- [37] U.R. Felscia, B.J.M. Rajkumar, M. Nidya, P. Sankar, Electronic and Nonlinear Optical Properties of L-Histidine on Silver: A Theoretical and Experimental Approach, *J. Phys. Chem. A* 122 (4) (2018) 1045–1052, <https://doi.org/10.1021/acs.jpca.7b07493>.
- [38] J.F. Dobson, T. Gould, Calculation of dispersion energies, *J. Phys.: Condens. Matter* 24 (2012) 073201, <https://doi.org/10.1088/0953-8984/24/7/073201>.
- [39] S. Lakhera, M. Rana, K. Devlal, Utilization of Methylthiazide Adsorbed with Malonamide for Quantum Chemical applications: A DFT and DFT-D2/D3 Studies, *Optik* 295 (2023) 171485, <https://doi.org/10.1016/j.joee.2023.171485>.
- [40] T. Koopmans, Ordering of wave functions and eigen energies to the individual electrons of an atom. *Physica*. 1 (1933) 104–113.
- [41] S. Lakhera, K. Devlal, M. Rana, V. Dhuliya, Influence of the substitution of different functional groups on the gas sensing and light harvesting efficiency of zero-dimensional coronene quantum dot: A first principle DFT study, *Spectrochim. Acta A Mol. Biomol. Spectrosc.* 308 (2024) 123737, <https://doi.org/10.1016/j.saa.2023.123737>.
- [42] D.E. Glendenning, C.R. Landis, F. Weinhold, Natural Bond Orbital Methods. 2 (1) (2012) 1–42, <https://doi.org/10.1002/wcms.51>.
- [43] E.D. Glendenning, C.R. Landis, F. Weinhold, NBO 6.0: Natural bond orbital analysis program, *J. Comput. Chem.* 34 (16) (2013) 1429–1437, <https://doi.org/10.1002/jcc.23266>.
- [44] Lu. Tian, F. Chen, Multiwfn: A Multifunctional Wavefunction Analyzer, *J. Comput. Chem.* 33 (2012) 580–592, <https://doi.org/10.1002/jcc.22885>.
- [45] N.M. Boyle, A.L. Tenderholt, K.M. Langner, *J. Comp. Chem.* 29 (2008) 839–845.
- [46] T. Hansson, J. Marelius, J. Åqvist, Ligand binding affinity prediction by linear interaction energy methods, *J Comput Aided Mol Des.* 12 (1998) 27–35, <https://doi.org/10.1023/A:1007930623000>.
- [47] S. Lakhera, K. Devlal, A. Ghosh, M. Rana, Modelling the DFT structural and reactivity study of feverfew and evaluation of its potential antiviral activity against COVID-19 using molecular docking and MD simulations, *Chem. Pap.* 76 (2022) 2759–2776, <https://doi.org/10.1007/s11696-022-02067-6>.
- [48] S. Lakhera, M. Rana, K. Devlal, I. Celik, R. Yadav, A comprehensive exploration of pharmacological properties, bioactivities and inhibitory potentiality of luteolin from *Tridax procumbens* as anticancer drug by in-silico approach, *Struct. Chem.* (2022), <https://doi.org/10.1007/s11224-022-01882-7>.
- [49] S. Lakhera, M. Rana, K. Devlal, N. Kanagathara, J. Janczak, Photovoltaic Characteristics of Organic Heterocyclic 2,9-dimethyl Quinacridone in Different Solvents Using DFT Approach, *J. Photochem. Photobiol. A Chem.* (2023) 114664, <https://doi.org/10.1016/j.jphotochem.2023.114664>.
- [50] S. Lakhera, M. Rana, K. Devlal, Comprehensive quantum chemical study of the associative complex of para-aminobenzoic acid and 7-diethylamino 4-methyl coumarin by adsorption and aromatic bridges, *J. Mol. Model* 30 (2024) 37, <https://doi.org/10.1007/s00894-023-05816-w>.
- [51] S. Lakhera, M. Rana, K. Devlal, S. Sharma, P. Chowdhury, V. Dhuliya, S. Panwar, Sagar L.P. Purohit, A. Dhanusha, T.C. Girisun, Exploring the Nonlinear Optical Limiting Activity of Para-Aminobenzoic Acid by Experimental and Dft Approach, *J. Photochem. Photobiol. A Chem.* (2023) 114987, <https://doi.org/10.1016/j.jphotochem.2023.114987>.